Underpotential deposition of Nickel on platinum single crystal electrodes

Francisco J. Sarabia, Victor Climent, Juan M. Feliu

PII: S1572-6657(17)30811-1
DOI: doi:10.1016/j.jelechem.2017.11.033
Reference: JEAC 3663

To appear in: *Journal of Electroanalytical Chemistry*

Received date: 14 August 2017
Revised date: 16 October 2017
Accepted date: 11 November 2017

Please cite this article as: Francisco J. Sarabia, Victor Climent, Juan M. Feliu , Underpotential deposition of Nickel on platinum single crystal electrodes. The address for the corresponding author was captured as affiliation for all authors. Please check if appropriate. Jeac(2017), doi:10.1016/j.jelechem.2017.11.033

Underpotential deposition of Nickel on platinum single crystal electrodes.

Francisco J. Sarabia, Victor Climent*, Juan M. Feliu*

Instituto Universitario de Electroquímica, Universidad de Alicante, Carretera San Vicente del Raspeig s/n, E-03690, San Vicente del Raspeig, Alicante, Spain

Abstract:

The initial stages of nickel electrodeposition on platinum single crystal electrodes have been investigated using cyclic voltammetry and CO charge displacement. While at pH=1, nickel deposition is not visible in the voltammogram, regardless of the crystal orientation, at buffered solutions with pH>3, nickel presence in solution produces clear voltammetric peaks around 0.35 V RHE on Pt(111) and Pt(110). Conversely, no clear voltammetric peaks are observed at any of the studied pHs on Pt(100). CO charge displacement experiments suggest that deposited nickel is in the form of a nickel hydroxide. Coulometric analysis is used to deduce the stoichiometry of the deposited adlayer. Moreover, the effect of nickel presence on CO oxidation have been investigated and the CO adlayer characterised using FTIR reflection absorption spectroscopy.

Keywords: Nickel deposition, platinum single crystal, FTIR spectroscopy, cyclic voltammetry, carbon monoxide, charge displacement

*Corresponding authors: Victor Climent: victor.climent@ua.es

Juan Feliu: juan.feliu@ua.es

Introduction:

There is significant interest in the modification of electrode surfaces by foreign metal adatom deposition to improve their catalytic activity. There are different reasons why those bimetallic surfaces exhibit enhanced activity [1, 2]. In some cases, the foreign element alters the electronic properties of the substrate. Such effects are usually parametrised in terms of the caused d-band shift in the density of states of the metal [3]. In other cases, the foreign adatoms add new reactive sites necessary for the reaction to take place. This is usually the case in the oxidation of organic molecules, also for carbon monoxide, that require a suitable source of oxygen [4]. Those reactions can benefit from the modification of the surface by hydrophilic adatoms, with a higher tendency to adsorb OH or O, resulting in what is usually called a bifunctional mechanism. Even inert adatoms can be beneficial for some reactions by blocking surface sites that may be detrimental for the reaction of interest, usually because they hinder undesired parallel reactions in the so called third body effect [5, 6].

Among the different methods available for the modification of electrode surfaces with metal adatoms, electrochemical deposition offers simplicity and high degree of control and accuracy. In many cases, the first (and sometime the second) layer of the deposited metal is formed at an electrode potential significantly more positive than the Nernstian potential for the bulk deposition [7]. This phenomenon has been coined with the term underpotential deposition (upd) and it is due to the existence of a stronger interaction energy between the adatom and the substrate than between the adatoms themselves in the bulk phase. In those cases, adatom coverage can be controlled with the electrode potential in the submonolayer amount with high precision, since there is a well-defined correspondence between coverage and potential. Anion adsorption plays in upd processes a very important role, not only because anions compete for surface sites with the deposited metal but also because anions can adsorb on the metal adlayer, therefore changing the energy of adsorption [8].

Bimetallic surfaces composed of Ni and Pt have received a lot of attention recently for their exceptional activity in the oxygen reduction (ORR) and the hydrogen evolution reactions (HER). $Pt_3Ni(111)$ alloys have been reported to exhibit the highest activity for ORR [9]. Deposition of small amounts of $Ni(OH)_2$ on Pt(111) surface has been shown to significantly reduce the overpotential for HER and Hydrogen oxidation reactions (HOR) in alkaline solutions [10, 11]. Recently, It has been pointed out that this effect might be related with changes in the potential of zero charge, since charge separation at the interphase affects reorganization energy of interfacial water [12]. Deposition of $Ni(OH)_2$ in alkaline solution is an irreversible process and coverage of the resulting adlayer is difficult to control. Conversely, nickel deposition in acid solution is hampered by the competition with the reaction of hydrogen evolution. Therefore, solution pH needs careful adjusting to achieve optimal conditions for nickel deposition. Ideally, one would like to deposit nickel in neutral or slightly acidic solutions and then transfer the modified electrode to alkaline solutions where the adlayer remains in a broad potential range.

Nickel upd was initially described on polycrystaline platinum [13, 14]. The upd process is overlapped with the hydrogen adsorption and evolution reaction what makes difficult its study. The Ni upd on single crystal electrode surfaces was attempted later an concluded that from the three basal planes the most clear upd process was observed on Pt(110) [15]. In

consequence, Ni upd on Pt(110) was further studied by cyclic voltammetry, and quartz crystal microbalance [16-18]. The effect of nickel adlayer on CO oxidation was also investigated for this surface [16]. However, to the best of our knowledge, very little information exist about nickel upd on Pt(111).

In this work we report a comprehensive electrochemical study of the initial stages of nickel deposition on Pt(111) and its effect on hydrogen adsorption and CO oxidation. For this purpose, we have used a combination of cyclic voltammetry, CO charge displacement and spectroscopic measurements.

Experimental:

Working electrodes were prepared from small beads, ca. 2 mm in diameter, obtained by the method described by Clavilier et al. [19, 20]. Prior to each experiment the working electrodes were flame annealed in a propane-oxygen flame, cooled down in a hydrogen/argon (1:3) atmosphere and transferred to the cell protected by a drop of ultra-pure water saturated with these gases [20].

The experiments were performed at room temperature in a classical three electrode cell configuration using a Luggin capillary to separate the reference electrode from the main working solution. A coiled platinum wire was used as counter electrode while a reversible hydrogen electrode (RHE) was used as reference. The Luggin capillary was filled with the same solution as that of the main compartment of the cell. The working electrode was contacted with the solution in the hanging meniscus configuration.

Solutions were prepared using concentrated perchloric acid (Merck Suprapur), sodium fluoride (Merck Suprapur) and ultrapure water from Elga Purelab Ultra Analytic system (Resistivity 18.2 MΩcm). Sodium sulfate, nickel perchlorate and nickel sulfate were also used to add nickel (II) or sulfate to the solution (Sigma-Aldrich). Argon, hydrogen and CO (N50, Air liquide) were used for deaerating the solution, to cool down the electrode after the flame annealing and for the CO displacement experiments. Solutions were deaerated by bubbling Ar for at least 15 minutes and during the experiments an Ar blanket was maintained above the solution to prevent the entrance of O_2 into the cell. Voltammetric curves were recorded with a signal generator (PAR 173), a potentiostat (Edaq EA161) and a digital recorder (eDAQ, ED401). The pH of the solution was measured using a PH-basic-20 pH-meter from Crison coupled with a pH-probe pH 50 12 HACH model

CO displacement experiments were performed by following the same methodology previously reported [21]. The experiment consists in the following steps: i) After recording the voltammogram, potential cycling was stopped at 0.1 V. When nickel is in solution, the polarization time at this potential was carefully controlled since it has an influence on the amount of deposited nickel. Ii) A suitable flow of CO was introduced into the electrochemical cell while the transients current, produced in response to the introduction of this gas, was recorded. During this step attention was paid to avoid the entrance of O_2 into the cell or the presence of O_2 traces in the CO flow. For this, all conductions were permanently flushed with either Ar or CO to avoid the permeance of O_2 through the walls of the tube. Iii) When current

decays to zero, indicating surface saturation, the CO flow was stopped and the excess CO in the solution and the cell atmosphere was removed by bubbling argon during ca. 10 minutes; iv) the surface blockage was checked in the low potential range previously to the stripping of the CO monolayer, which is achieved in a single sweep to a sufficiently high potential limit (0.85-0.9 V) ; iv) the recovery of the initial surface profile is then verified.

Some experiments with a flow cell were preformed to test the stability of nickel adlayers in the absence of nickel in solution. This cell is equipped with an outlet at the bottom and an inlet on top connected to a reservoir that allows removal of the electrolyte and its exchange with solution of different composition without losing the potential control of the working electrode. The reservoir is bubbled with Ar to ensure that the solution is always deaerated.

In situ external reflection infrared experiments were carried out with a Nicolet 8700 (Thermo Scientific) spectrometer equipped with a MCT-A detector using p-polarized light and with a spectral resolution of 8 cm^{-1}. The glass spectroelectrochemical cell was equipped with a prismatic CaF_2 window bevelled at 60°. A Ag/AgCl/KCl saturated electrode was used as reference in this case, but all potentials have been converted to the RHE scale for consistency. The Pt(111) working electrode used in these experiments was ca. 4.5 mm in diameter and was prepared and treated before experiments in a similar way as the smaller samples used in the voltammetric experiments. The spectra are plotted in absorbance units ($-\log(R/R_0)$) by referring the single beam reflectance spectrum collected at the sample potential (R) to the one collected at the reference potential (R_0). The reference potential was selected as 0.9 V for the study of the CO bands and 0.1 V for the study of the formation of CO_2 (see below).

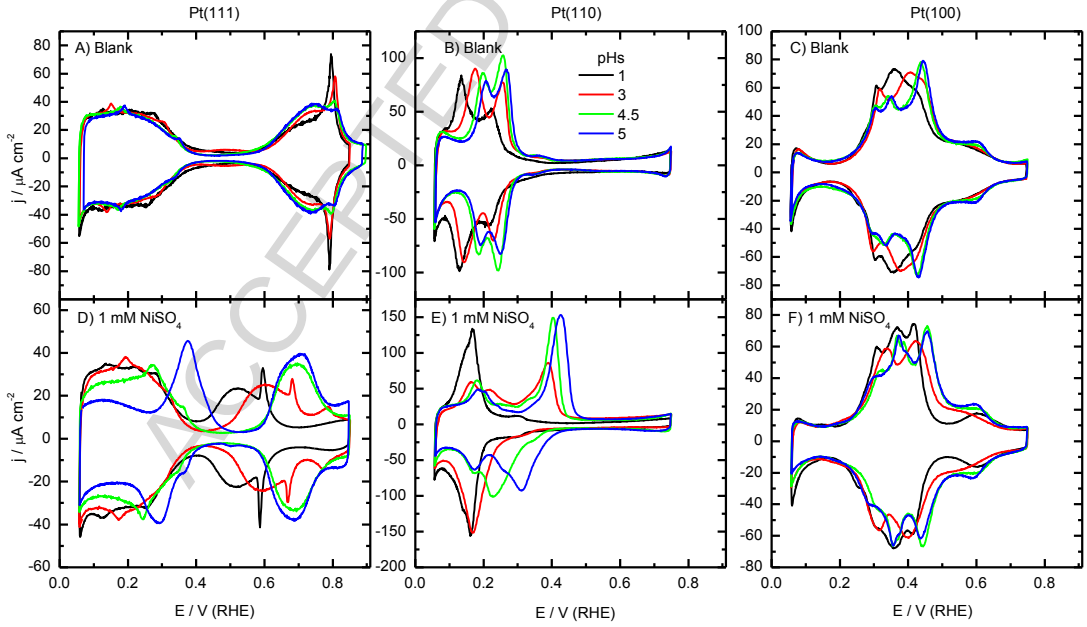

Figure 1. Cyclic voltammograms for Pt(111) (A,D), Pt (110) (B,E) and Pt(100) (C,F) electrodes in 0.1M $HClO_4$ (pH 1, black); and 0.1M $NaF/HClO_4$ mixtures of different pH: pH 3, red; pH 4.5, green and pH 5, blue. Top panels show the voltammograms without Ni^{2+} (A, B and C) and bottom panels the results with 1mM $NiSO_4$ (D,E and F). Scan rate: 50 mV/s.

Results and discussion:

Cyclic voltammetry

Figure 1 shows the voltammetric profiles for the Pt(111), Pt(110), and Pt(100) electrodes in differents pHs, with and without nickel in solution. The voltammograms recorded in the absence of nickel coincide with those previously reported in similar media. The characteristic features and the stability of the voltammograms upon cycling imply that the electrolyte solution is free of impurities. For the Pt(111) electrode in the absence of nickel, the small features around 0.15 V and 0.27 V can be ascribed to small amount of (110) and (100) defects, respectively. The small charge density under these peaks, together with the magnitude of the sharp peak at 0.80 V is a clear indication of the good quality of the electrode. The integrated charge involved in the hydrogen reductive adsorption (negative scan) and oxidative desorption (positive scan) zone (0.06 V – 0.4 V) decreases slightly from 160 $\mu C/cm^2$ to ca. 150 $\mu C/cm^2$, after double layer correction, when the pH increases from 1 to 5. Apart from this decrease, the current in this region remains nearly unaffected by the increase of the pH in the RHE scale [22, 23] (except for the shift of the small defect peaks). This means that all processes shift with the pH in the same extent as the reference electrode. The voltammetric region above 0.55 V corresponds to the oxidative adsorption (positive scan) and reductive desorption (negative scan) of OH ions. Changes in this region with the increase of the pH are more significant, with the broad peak around 0.74 V increasing and the sharp peak at 0.80 V decreasing. Again, peak potentials in this region do not shift with pH in the RHE scale. For Pt(110) electrode, the voltammetric curves show two peaks appearing below 0.3 V. These peaks correspond to the coupled desorption of hydrogen and adsorption of OH in the positive sweep and the reverse reactions in the negative sweep. In this case, the peaks shift towards positive potentials with the increase of the pH in the RHE scale. This shift means that they move with the pH less than the reference electrode. Similar effects are observed for Pt(100). In this latter case, the voltammogram contains several peaks that shift differently with the variation of the pH [24]. The processes at lower potentials are usually ascribed to (mainly) hydrogen adsorption / desorption while the broad voltammetric peak around 0.6 V is ascribed to OH adsorption. The small peaks around 0.3-0.35 V are due to the small presence of steps. Those steps are generated as consequence of the lifting of the reconstruction [25, 26]. The latter is created during the flame annealing step and it is removed when the electrode is contacted with the solution [27].

When nickel sulfate is added to the solution, significant changes are observed in the voltammograms recorded with Pt(111) and Pt(110) while the voltammogram corresponding to Pt(100) changes only slightly. The effect of nickel is more visible at the highest pH, while no effect is observed at pH=1 for any of the surfaces. For Pt(111) and Pt(110) the voltammograms show a rather irreversible (asymmetric) redox pair around 0.3/0.4 V vs RHE. This redox pair is clearly visible for the two electrodes at pH 5 while for lower pH values it is only visible for Pt(110). This result is in accordance with previous reports [15] (while a small peak corresponding to nickel stripping from Pt(110) was reported in [15] at pH=1 when the scan rate is 2mV/s, we could not observe any peak under the present experimental condition at this pH, most likely due to the faster scan rate, 50 mV/s). Other changes in the voltammogram can be easily related to the presence of sulfate counterions. In particular, for Pt(111) at the lowest pH, the OH adsorption region is replaced by clear sulfate adsorption peaks around 0.5 V [28].

In this case, the sharp spike at 0.58 V corresponds to the sulfate disorder-order phase transition to give the $(\sqrt{3}\,x\,\sqrt{7})R19.1^0$ structure characteristic of sulfate adsorbed on this surface [29, 30]. As pH increases, these peaks decrease, while the waves associated with the adsorption-desorption of hydroxyl ions increase. As will be shown below, nickel presence has also some effect on the OH adsorption region.

For Pt(110) electrode at pH 1 with $NiSO_4$, a reversible peak is observed at 0.15 V corresponding to the coupled hydrogen, hydroxyls and sulfates ions adsorption-desorption processes. No sign of Nickel deposition is observed at this concentration. When the pH increases, the corresponding charge of these processes decreases, favoring the nickel adsorption. At pH 3 the cathodic peak at 0.17 V corresponds to nickel adsorption overlapped with proton adsorption and anions desorption processes. The anodic peak at 0.37 V corresponds to the oxidation of the adsorbed nickel species. For pHs 4.5 and 5, the peaks related with proton and anion adsorption-desorption and the redox peak corresponding to nickel interaction with the surface are well separated. For Pt(100) electrode there are no clear peaks that suggest nickel adsorption at these pH values and most changes in the voltammogram can be attributed to the presence of sulfate counter-anion.

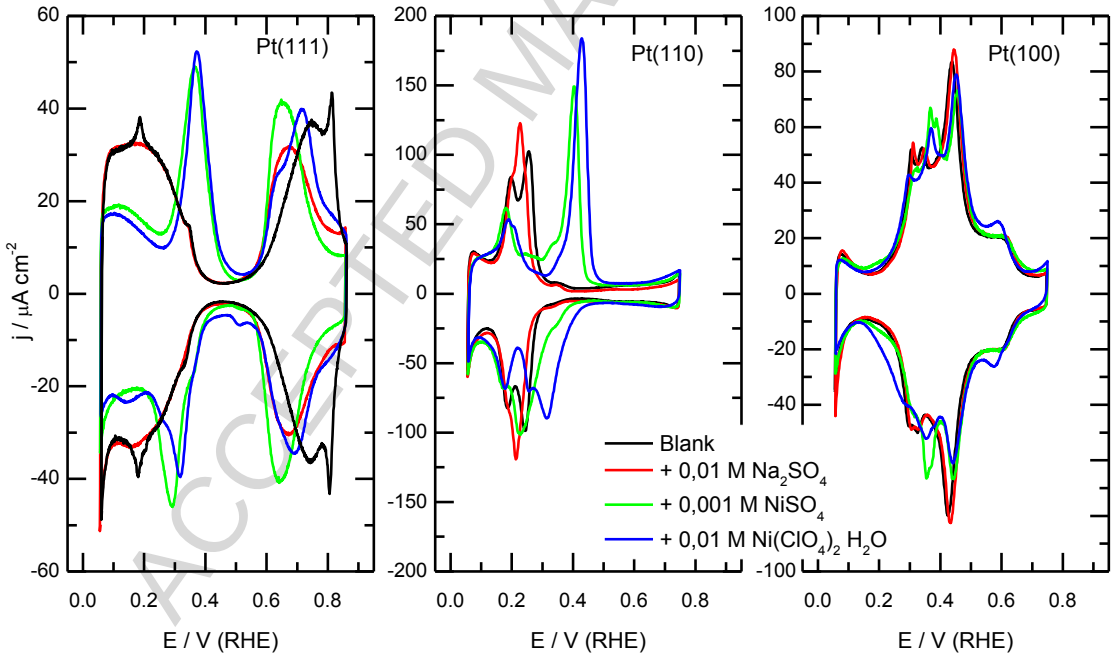

Figure 2. Cyclic voltammograms for Pt(111), Pt(110) and Pt(100) electrodes in a 0.1 M NaF/$HClO_4$ mixture (pHs 4.5) (black curve) and with 10 mM $NiSO_4$ (green), 10 mM Na_2SO_4 (red) and 10 mM $Ni(ClO_4)_2$ (blue). Scan rate: 50 mV/s.

To separate the effect of nickel from the effect of sulfate on the high potential region of the voltammogram, additional experiments were performed using nickel perchlorate and sodium sulfate. Figure 2 shows the corresponding results, at pH 4.5. For Pt(111) in the absence of

nickel and sulfates, the peak of hydroxyl adsorption appears at 0.75 V (black curve). The addition of sodium sulfate to the solution (red curve) causes a shift of this peak by around 80 mV towards less positive potentials (0.67 V). On the other hand, the addition of nickel perchlorate (blue curve), besides the pair of peaks at 0.3/0.4 V already discussed, also causes a clearly discernible shift in the OH region. The effect of cations on this potential region has already been reported [31, 32]. One plausible explanation for this effect lies on the interaction of the cations with the first water layer in contact with the electrode surface, altering the network of hydrogen bonds. In this regards, the structure forming or structure breaking properties of ions were used to explain the effect of small concentration of ions on this region of the Pt(111) voltammogram [33]. The contribution of both ions, sulfate and nickel, (green curve) generates a larger displacement with a difference of 100 mV with respect to the blank.

For Pt (110), the presence of sulfate affects the peaks that appear at 0.2 V and 0.25 V, where the hydrogen, hydroxyls and sulfate adsorption and desorption processes take place. In the presence of nickel perchlorate (blue curve), a decrease in the charge associated with these processes is observed due to the electrode surface occupation by the nickel. At Pt(100) electrodes no significant differences were observed between the voltammograms in the presence and absence of sodium sulfate or nickel perchlorate.

In the following, from the three basal planes, we focus on Pt(111) for the following reasons: i) Clear effect of the presence of nickel is observed on this surface ii) hydrogen and nickel adsorption processes are well separated from hydroxyl and anion adsorption region, allowing a quantitative analysis of the voltammetric charges and iii) nickel interaction with Pt(110) has already been reported [15, 17, 18, 34]. Because results of figure 2 prove that effect of sulfate is only marginal, the following experiments were carried out with nickel sulfate as the source of nickel ions in the solution because of the higher purity of this salt.

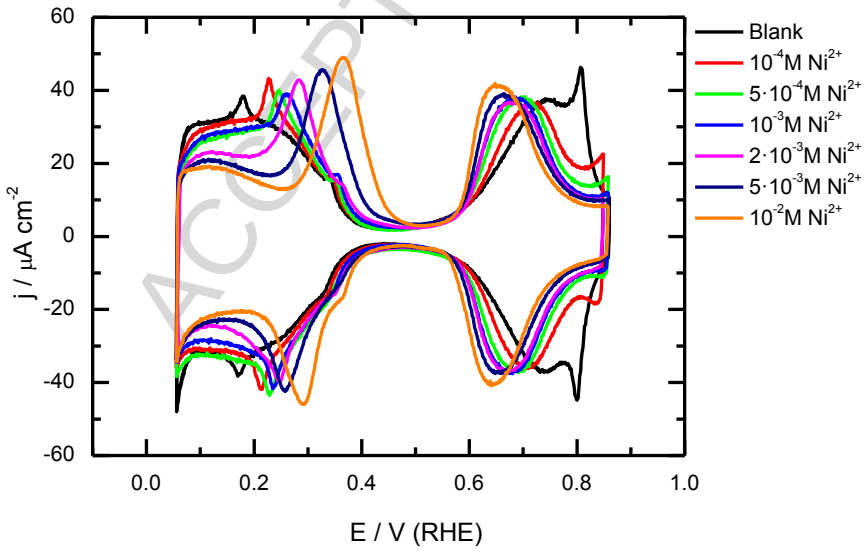

Figure 3. Cyclic voltammograms for Pt(111) in 0.1M NaF/$HClO_4$ (pHs 4.5) with different nickel sulfate concentrations, as indicated in the figure. Scan rate: 50 mV/s

The effect of nickel concentration on the voltammogram of Pt(111) is shown in Figure 3. While the presence of nickel is already discernible at the lowest concentration, its effect at this pH is clearer for concentrations above 10^{-3} M. More information can be obtained from the integration of charges. To avoid any ambiguity in the selection of the base line that separates nickel from hydrogen processes, total charges in this region were integrated between 0.06 and 0.5 V. The integrated charge involved in the hydrogen adsorption-desorption region is the same for all concentrations (~155 μC/cm^2). To correct the capacitive contribution to this charge, the voltammetric current in the double layer region around 0.5 V was subtracted prior to the integration.

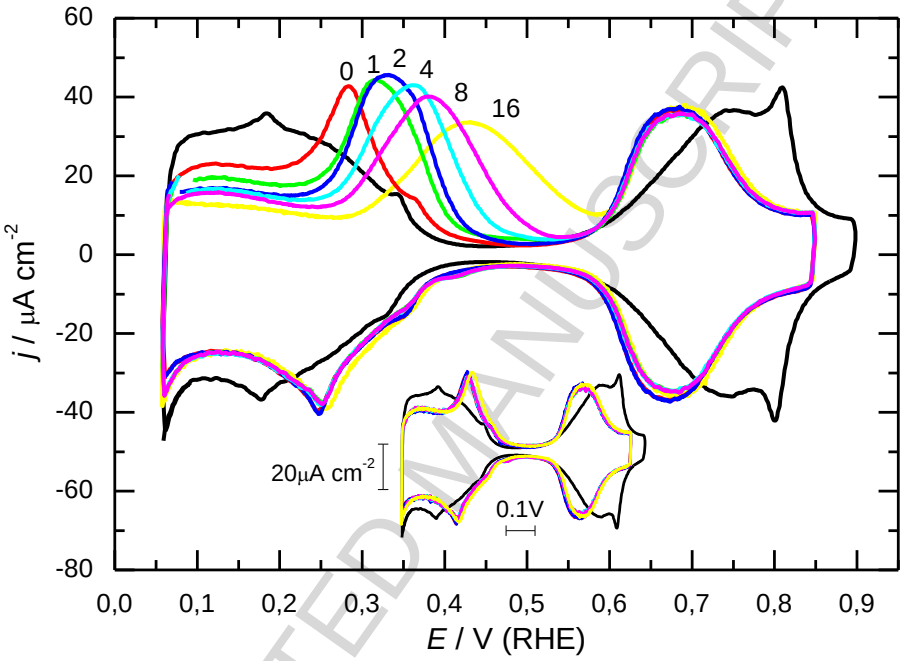

Figure 4. Cyclic voltammograms for a Pt(111) electrode in 40 mM NaF/$HClO_4$ (pHs 4.5) with 2mM $NiSO_4$, after holding the working electrode for different times at 0.1 V. labels indicate the time in minutes. Scan rate: 50 mV/s. The inset shows the second scan for each case.

***t* (min)**	***q* (μC/cm^2)**
1	153
2	153
4	156
8	160
16	149

Table 1. Integrated charge involved in the low potential region for the voltammograms of figure 4, corresponding to different nickel deposition times.

Figure 4 shows the first voltammetric scan after holding the potential at 0.1V vs RHE for different times, in pH 4.5 with 2mM nickel sulfate. The peak assigned to nickel becomes broader and shifted to higher potentials with the increase of the holding time. The total integrated charge involved in hydrogen adsorption-desorption and nickel oxidation-reduction region is the same in all cases (~155 μC/cm^2, see table 1). The inset in Figure 4 shows the

second scans for each deposition time. In all cases, the initial voltammogram is recovered at the second scan, identical to the one recorded for continuous cycling of the potential. So, the peak displacement observed in the main figure 4 is clearly related to the holding time.

CO charge displacement

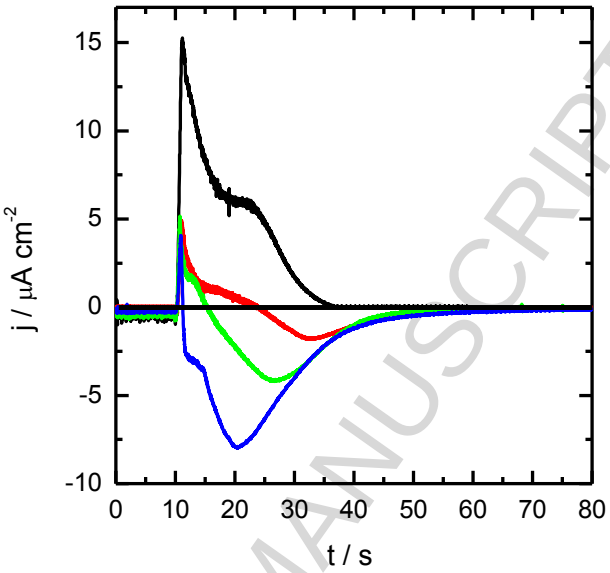

Figure 5: CO displacement at 0.1 V RHE, in 40 mM $NaF/HClO_4$ pH 4.5, with different nickel concentration and holding time at 0.1 V: in absence of nickel (Black); $5 \cdot 10^{-4}$M nickel sulfate, 3.5 min (red); $5 \cdot 10^{-4}$M nickel sulfate, 16.5 min (green) and 10^{-2}M nickel sulfate, 3.5 min (blue).

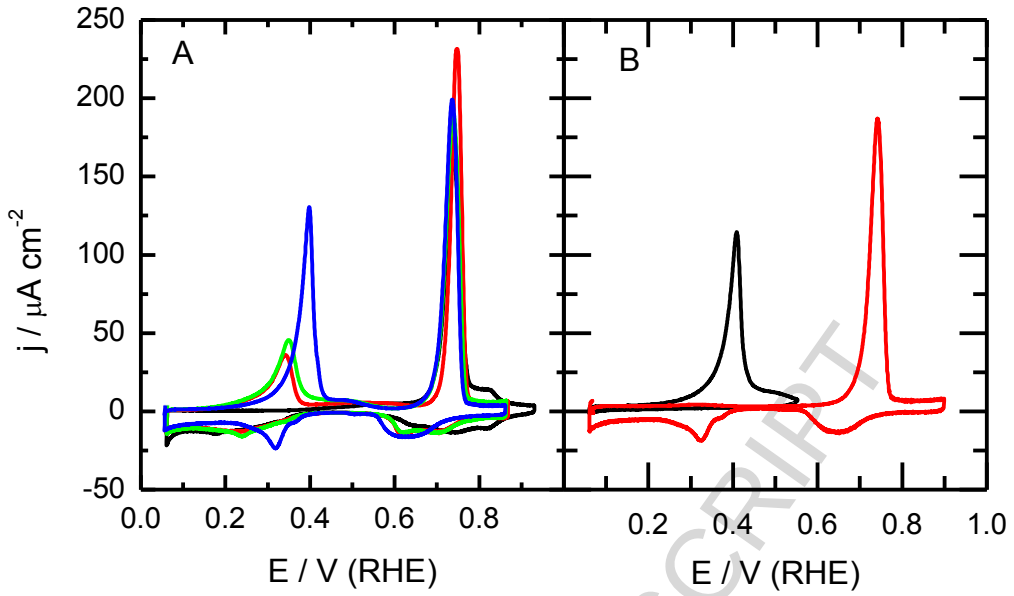

Figure 6. A) CO stripping after the CO displacement experiments reported in figure 5. B) Effect of reversing the potential scan after the first peak. Scan rate: 20 mV/s.

As discussed in previous paragraphs, one of the difficulties in the quantitative analysis of the voltammetric charges is the overlap between hydrogen and nickel associated processes. To try to separate both contributions, CO displacement experiments were performed with Pt(111) in nickel containing solutions. In this experiment, the current flowing during the potentiostatic adsorption of CO is recorded as a function of time. Figure 5 shows the curves *j* (μC/cm^2)-*t* (s) obtained in the CO displacement for Pt(111) electrode at pH 4.5, in presence and absence of nickel in solution. In all cases the holding potential was 0.1 V. In the absence of nickel, a positive current is observed during CO adsorption due to the displacement of hydrogen. The integrated charge involved in CO displacement for this case amounts to 140 μC/cm^2 at 0.1 V vs RHE, in accordance with previous reports [22]. The same experiment was repeated with different nickel coverages. To change the amount of deposited nickel, the nickel concentration in solution and the holding time was varied. As shown in figure 5, as the nickel coverages increases, a negative contribution to the current appears during CO displacement, while the positive contribution decreases. The displacement of nickel according to:

$$Pt\text{-}Ni + CO \rightarrow Pt\text{-}CO + Ni^{2+} + 2e \qquad (1)$$

would produce positive current and therefore this reaction is not in agreement with the experimental result. The negative charge suggests the presence of an adsorbed anion that is displaced by CO. Since the voltammogram in the low potential region is not affected by the presence of sulfate, we propose that this anion is OH adsorbed on the nickel adatoms. Therefore, the displacement reaction in the presence of nickel would be:

$$Pt\text{-}Ni\text{-}(OH)_n + CO \rightarrow Pt\text{-}Ni\text{-}CO + n\ OH^- + n\ e \qquad (2)$$

For the maximum nickel coverage the charge displaced amounts to -130 μCcm^{-2}. CO displacement has been previously used to determine the potential of zero total charge (pztc) of platinum electrodes. For Pt(111) the pztc is located around 0.55 V RHE at pH=4.5 in the double layer region. The recorded negative values of displaced charge for the nickel covered surface indicates that the pztc is located at potentials lower than 0.1 V. This implies a significant displacement of the pztc as a consequence of the nickel deposition. Unfortunatelly, the exact location of the pztc is not accessible from the combination of the displaced charge and the integration of the voltammogram [23, 35-37] because the interference of hydrogen evolution and bulk nickel deposition. It is also worth pointing out that nickel electrosorption valency on polycrystaline platinum has been reported from EQCM measurements to be significantly lower than 2 [18, 34]. Hydroxyl coadsorption on the nickel adatoms clearly supports this result.

Additional clues to understand the nature of nickel on the surface are obtained from the oxidation of the CO adlayer resulting from the displacement process, after removing the excess CO in the solution. As shown in figure 6A, the curve for the CO stripping contains two well separated peaks, the first at around 0.35 V and the second at 0.75 V. The second peak coincides in potential and charge with the one recorded in the absence of nickel, and therefore can be ascribed to the oxidation of the CO adsorbed on platinum. What is striking about this peak is that its charge remains nearly independent of the amount of nickel deposited at the low potential end. On the other hand, the first peak increases in magnitude as it does the amount of nickel deposited on the surface. Therefore, this peak should be ascribed to the oxidation of nickel, although it may also contain a small contribution from the oxidation of CO adsorbed on nickel. Further understanding of the nature of this peak is obtained from the experiment reported in figure 6B. In this case, after the first peak is completed, the potential scan was reversed. Remarkably after the first oxidation peak no surface is freed as deduced from the low voltammetric current recorded in the second cycle between 0.06 and 0.5 V. This indicates that negligible amount of CO is oxidised in the first peak and therefore this peak should be ascribed mainly to the oxidation of nickel. Similar conclusions were already proposed for the case of Pt(110) [34]. We cannot exclude the oxidation of a small amount of CO if we take into account that different CO structures can produce total blockage of the surface [38]. In this regards, it has been reported that partial oxidation of CO adlayers in the so-called prewave region does not free surface sites since a reorganization (expansion) process in the CO adlayer takes after the partial oxidation [39].

Coulometric analysis

By analyzing the transient charges involved in the CO displacements, we can calculate the nickel contribution. During the CO displacement with nickel sulfate in solution, two contributions participate in the net current recorded, a positive contribution produced by the displacement of the remaining hydrogen, after nickel adsorption:

$$q_H = q_{H,0.1}^{\theta=0}(1 - m\theta_{Ni}) \qquad (3)$$

and a negative contribution due to displacement of the OH adsorbed on nickel

$$q_{OH} = n\, q_{111}\theta_{Ni} \qquad (4)$$

Where $q_{H,0.1}^{\theta=0}$ is the hydrogen charge on the blank experiment recorded at 0.1 V in the absence of nickel (140 μC/cm^2), q_{111} is the charge corresponding to one electron per Pt atom on the (111) surface (240 μC/cm^2), *n* is the number of OH species per nickel (the stoichiometry OH/Ni) and *m* is the number of Pt atoms blocked by each nickel adatom. Therefore, the displaced net charge (q_{net}^{d}) is the difference between the positive and negative contributions. It can be expressed by the equation:

$$q_{net}^{d} = q_{H,0.1}^{\theta=0}(1 - m\theta_{Ni}) + (-n\, q_{111}\theta_{Ni}) \qquad (5)$$

Therefore:

$$\theta_{Ni} = \frac{q_{H,0.1}^{\theta=0} - q_{net}^{d}}{q_{H,0.1}^{\theta=0} m + q_{111} n} \qquad (6)$$

Because there are two unknowns in this equation (*n* and *m*) we cannot calculate nickel coverage from the displaced charges, yet. To get additional information, we need to consider again the voltammetric charges, considering the presence of adsorbed OH. When the potential is scanned from 0.06 V towards positive values, the following processes will take place:

$$H \rightarrow H^{+} + e^{-} \qquad (7)$$

$$Ni \rightarrow Ni^{2+} + 2e^{-} \qquad (8)$$

$$OH + e^{-} \rightarrow OH^{-} \qquad (9)$$

Each process will contribute to the voltammetric charge according to the following equations:

$$q_{H} = q_{H,0.06}^{\theta=0} \cdot (1 - m\theta_{Ni}) \qquad (10)$$

$$q_{Ni} = q_{111} \cdot 2\, \theta_{Ni} \qquad (11)$$

$$q_{OH} = -n\, q_{111}\theta_{Ni} \qquad (12)$$

Where $q_{H,0.06}^{\theta=0}$ is the hydrogen charge in the blank voltammogram integrated from the double layer to 0.06 V. The total voltammetric charge is the result of the addition of the three contributions above:

$$q_{tot} = q_{H,0.06}^{\theta=0} + \left[-q_{H,0.06}^{\theta=0} m + q_{111}(2 - n)\right]\theta_{Ni} \qquad (13)$$

Since the experimental observation from the results reported in figures 3 and 4 is that the total voltammetric charge is independent of the amount of deposited nickel, the term $\left[-q_{H,0.06}^{\theta=0} m + q_{111}(2 - n)\right]$ in equation (13) must be zero. In this way, we obtain the following relation between *m* and *n*:

$$m = \frac{q_{111}}{q_{H,0.06}^{\theta=0}}(2 - n) \qquad (14)$$

Combining the equations 2 and 7 it turns out that nickel coverage (θ_{Ni}) can be calculated from:

$$\theta_{Ni} = \frac{q_{H,0.1}^{\theta=0} - q_{net}^{d}}{q_{H,0.1}^{\theta=0} \frac{q_{111}}{q_{H,0.06}^{\theta=0}}(2-n) + q_{111} n} \qquad (15)$$

If we neglect the small difference between $q_{H,0.1}^{\theta=0}$ and $q_{H,0.06}^{\theta=0}$ (ca. 10 μC/cm^2) equation (15) becomes independent of *n*:

$$\theta_{Ni} = \frac{q_{H,0.1}^{\theta=0} - q_{net}^{d}}{2\, q_{111}} \qquad (16)$$

In conclusion, nickel coverage can be calculated from the displaced charge. This analysis also neglects the double layer charge that should be added to equation (5). This charge is typically an order of magnitude smaller that the charge involved in adsorption processes and therefore this assumption is reasonable. Nickel coverages calculated in this way will be compared in the next section with the charge of the first peak recorded during CO oxidation

Analysis of CO stripping charges

Finally, we analyze the charges for the CO stripping. As previously discussed, the charge in the first stripping peak, q_{strip}^{1}, is mainly due to the oxidation of the nickel adatoms [34]. We consider also the possibility of a small amount of CO oxidation in this peak:

$$q_{strip}^{1} = 2 \times q_{111} \times \theta_{Ni} + q_{CO}^{1} \quad (17)$$

Where the first term accounts for the charge due to nickel oxidation and q_{CO}^{1} is the charge corresponding to the CO oxidation. To test the validity of the previous assumptions, we plotted in figure 7 the ratio:

$$\frac{q_{strip}^{1}}{q_{111}\theta_{Ni}} = \frac{2q_{strip}^{1}}{q_{H,0.1}^{\theta=0} - q_{net}^{d}} \qquad (18)$$

as a function of the nickel coverage, as obtained from equation (16). If the amount of CO oxidised in the first peak (q_{CO}^{1}, in equation (17)) were negligible, this ratio should give a constant value of 2. As expected this ratio approaches the value of 2 at high nickel coverages but deviates significantly from this value at low coverages. This means that CO oxidizes at very low potentials when the surface is partially covered with nickel, but little CO is oxidized when nickel is covering most of the surface. This seems to suggest that the active site for CO oxidation is the boundary between nickel islands and the uncovered platinum regions. In this case, the CO oxidation and nickel oxidation would take place in the same potential region and therefore, the amount of oxidized CO in the first peak would depend on the interplay between the rates of both processes. If nickel oxidizes too soon, there will be no nickel-platinum pairs that could catalyze the oxidation of CO. To further test these ideas, chronocoulometric experiments were performed, by stepping the potential either to the onset of the peak (0.22 V) or to well above the peak (0.50V). In the first case, lower oxidation charges are obtained (290 μCcm^{-2}), that we attribute mainly to nickel oxidation. In this case the driving force (overpotential) is not enough for the oxidation of CO and only (mainly) nickel is oxidized. On the other hand, if the potential is stepped to values higher than the peak, higher oxidation charges are obtained that must be ascribed to the coupled oxidation of nickel and CO.

Interestingly, the stripping curves after the potential step experiments show the main differences in the prewave region, while the main peak is nearly the same, except for the differences at high potentials, also visible in the voltammogram without CO, due to the presence of sulfate. It is worth noting the enhanced prewave at 0.48 V observed after the nickel oxidation at 0.22 V (black curve in figure 8). As explained before, and also postulated in [34], the CO that covers the nickel at low potentials is transferred to the platinum after nickel stripping. It is likely that such CO results in the formation of a less stable structure that gives such enhanced prewave. The origin of such prewaves has been controversial but it is usually ascribed to a relaxation in the CO adalayer resulting in a decrease in coverage most likely triggered at defects sites [40]. When the step potential is done at 0.50 V this less stable CO is oxidised and therefore the prewave is not visible. Hence, the formation of such less stable structure is most likely the reason for the different charges registered at 0.22 V and 0.50 V.

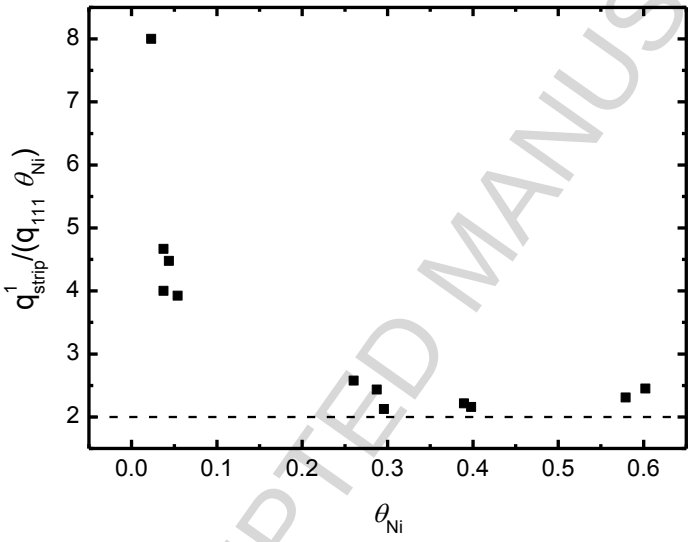

Figure 7. Ratio between the charge of first peak in the CO stripping and the corresponding charge for nickel stripping, as deduced from displaced charges, as a function of the nickel coverage.

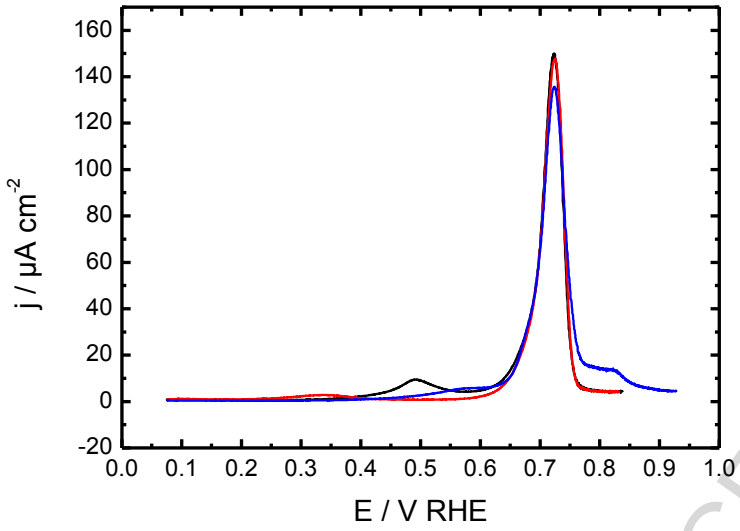

Figure 8: CO stripping curves after potential steps experiments at 0.22 V (red) and 0.50 V (black). The blue curve shows the blank experiment without nickel. Scan rate: 20 mV/s

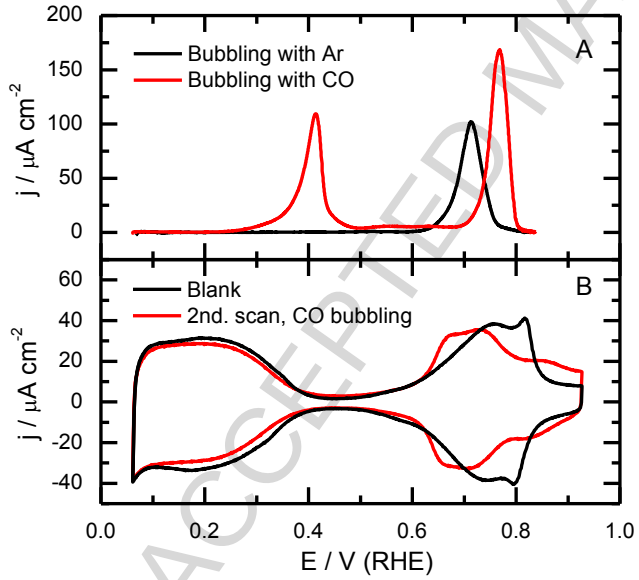

Figure 9: A) cyclic voltammograms recorded in a flow cell after exchanging the solution: initial solution was 40 mM NaF/$HClO_4$ pH 4.5 with 10 mM $NiSO_4$ and the final solution was 0.1 M NaF/$HClO_4$ pH 4.5 without nickel. During the exchange of solution the potential was held at 0.1 V. Prior to the solution exchange, CO was introduced to cover the electrode with adsorbed CO. During the exchange of the solution, it was bubbled with Ar (black) or CO (red). B) comparison between a blank voltammogram in solution without Ni with the second scan after the Ni stripping shown in figure A, when the exchange is done under CO bubbling.

Additional experiments were also done with a flow cell that allowed the exchange of the solution while keeping the potential control. The motivation for this experiment was to test the stability of nickel adlayer in a solution that does not contain Ni^{2+}. Such adlayer might be interesting for catalytic purposes. For this experiment, the electrode potential was held at 0.1 V for several minutes in a solution containing 10 mM $NiSO_4$. Then, the solution was exchanged with fresh electrolyte without Ni^{2+}, while keeping the potential at 0.1 V. After the exchange of the solution, the voltammogram was recorded. However, this voltammogram (not shown) did not show any evidence of nickel on the surface, indicating that nickel adsorption is reversible and as soon as nickel is removed from the solution, nickel from the surface is dissolved. Next, the effect of adsorbing CO on nickel stability was tested, to see if CO adsorption could improve the stability of nickel. The result in this experiment is shown in figure 9. In this case, CO was bubbled in solution while the potential was held at 0.1 V for several minutes. Then, solution was exchanged with a CO- and nickel-free solution. Again, the voltammogram recorded in this case (black curve in figure 9A) showed no signal of the presence of nickel. Finally, the experiment was repeated but this time maintaining the CO flux during all time that lasted the solution exchange. In this case, the peak at 0.4 V corresponding to nickel stripping from the CO covered suface is clearly visible. These experiments give a clear indication of the lability of nickel adsorption and the effect of CO on it. CO adsorption on Ni stabilizes the adlayer.

Spectroscopic investigation of the CO adlayers on nickel:

Characterization of the CO adlayers on nickel covered Pt(111) was also performed using FTIRRAS. To record these spectra, after introducing the electrode at the desired starting potential (0.1 V), CO was initially bubbled for 5 minutes to saturate the surface. Then, argon was bubbled to remove the CO from the solution and the electrode was pressed against the CaF_2 window, still holding the electrode potential at the initial value. Then, after recording an initial spectrum, the potential was sequentially stepped to increasing values and spectra were recorded at each potential until all the CO was oxidised. The spectra recorded with CO on the surface were referenced to the spectra recorded after CO oxidation. Therefore, positive bands correspond to the CO on the surface. These results are presented in panels B and D of figure 10. To analyse the formation of CO_2 which is a measure of the amount of CO oxidised, the spectra were also recalculated by referencing to the spectrum recorded at 0.06 V, where no CO_2 is present in the solution. In this case, CO_2 band appears as positive, as shown in panels A and C. On the Pt(111) without nickel two main CO bands are observed, at 2050 and 1825 cm^{-1} that can be ascribed to on top and bridge CO, respectively [41]. No band is observed for CO adsorbed on the hollow position, that should appear below 1800 cm^{-1}, as has been previously described at lower pHs [41], suggesting that only the $\sqrt{19}\,x\,\sqrt{19}$ structure is favored in this case, in the absence of CO in solution, instead of the c(2x2)3CO. Observation of the CO_2 band indicates that CO starts to oxidise at 0.47 V. This coincides with the small prewave in the voltammogram.

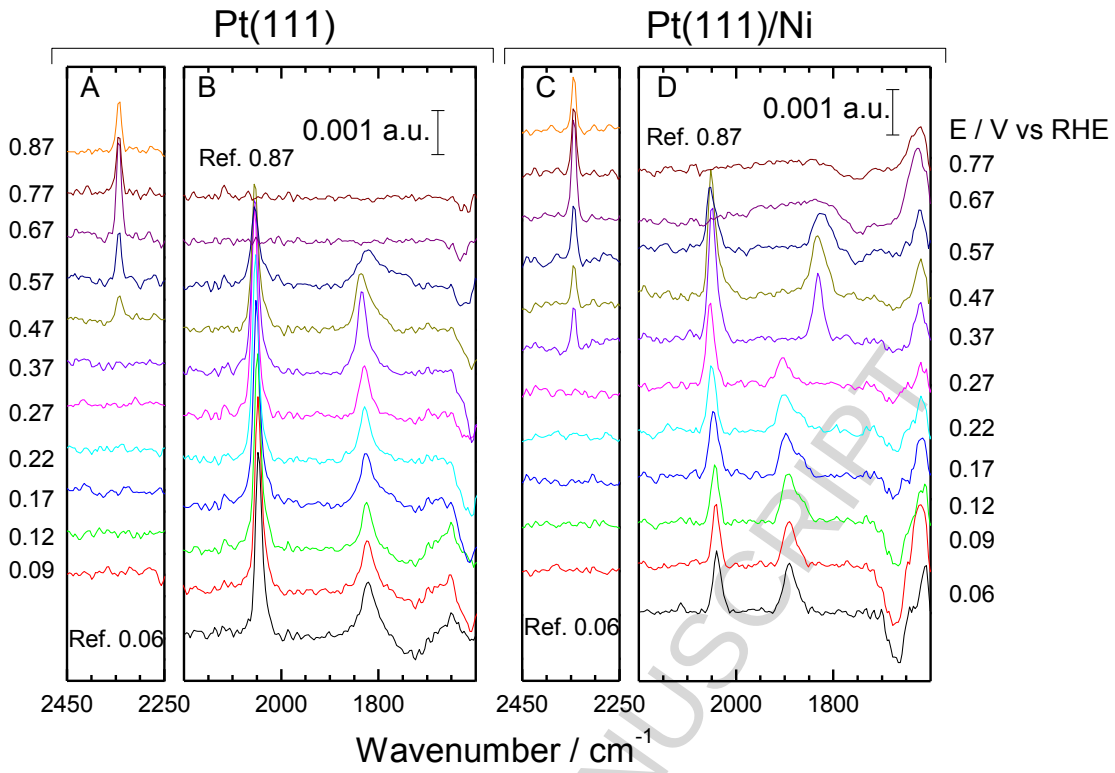

Figure 10: FTIR spectra recorded during CO oxidation on Pt(111) surface in 40 mM M $NaF/HClO_4$ solution, pH=4.5. A and B) no nickel in solution, C and D) 0.1 M $NiSO_4$. A) and C) show the CO_2 band after substracting as reference the spectra collected at 0.06 V. B) and D) show the CO bands after substracting as reference the spectra collected at 0.87 V i.e., after complete CO oxidation. 200 interferograms were collected at each potential.

When nickel is present on the surface, still two CO bands are observed at the lowest potential. The band corresponding to on top CO is still visible at the same wavenumbers but the band corresponding to bridge CO shifts to ca. 1900 cm^{-1}. For Ni(111) surfaces in alkaline media a single band at ca. 1900 cm^{-1} has been attributed to bridge CO [42], in accordance with UHV studies[43, 44]. Therefore, we ascribe the band at 1900 cm^{-1} to the CO adsorbed on Ni adatoms. When the potential is stepped above 0.3 V a sudden displacement of the band at 1900 cm^{-1} to the value characteristic for platinum, 1825 cm^{-1} can be observed. The onset for this transformation coincides rather well with the first voltammetric peak that has been ascribed before to the stripping of the nickel adalayer.

This transformation is linked with an increase of intensity of both bands for on top and bridge CO, that suggest that CO molecules that were on the nickel adatoms are transferred to the platinum when nickel is oxidised. We should remark here that band intensities are not a direct measure of the population of the corresponding oscillators, since they depend on a number of factors, like the orientation of the molecule and the coupling between adjacent oscillators. The latter is responsible of the phenomenon of intensity stealing from low energy bands to high energy bands [45]. For instance, this explains that the band corresponding to on top CO is more intense than bridge CO in the $\sqrt{19}\,x\,\sqrt{19}$ structure although the population of the later

is significantly higher [45, 46]. This may explain why with a surface that is mostly covered with nickel we still see a band at 2050 cm^{-1} that can be ascribed to CO adsorbed on top of the remaining platinum atoms. The CO_2 band is observed first at 0.37 V, a potential 100 mV lower than on the nickel free surface, indicating that small amount of CO oxidation takes place coupled with the nickel oxidation peak. All these trends can be more clearly seen in the plot of figure 11, where intensities of the different bands have been plotted as a function of the electrode potential. Bands corresponding to CO on Pt steeply increase coinciding with the voltammetric peak corresponding to nickel stripping. Another remarkable feature of this plot is that CO on nickel decreases at potentials well below the onset for the formation of CO_2. Both observations clearly support that CO on nickel is transferred to platinum before being oxidised.

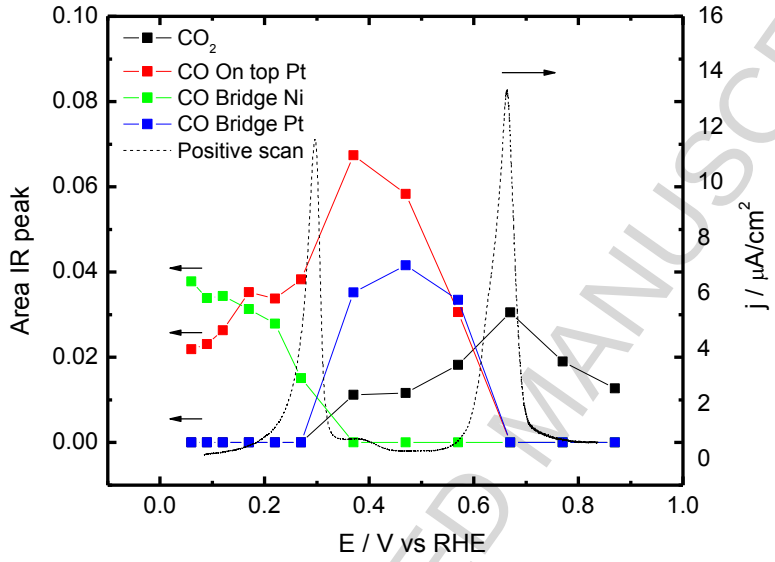

Figure 11: Plot of band intensities for CO adsorbed on Pt(111) covered with nickel in 40 mM $NaF/HClO_4$ solution, pH=4.5 containing 0.1 M $NiSO_4$. Dashed line represents the stripping voltammogram recorded under the same conditions at 2 mV/s

Concluding remarks

Nickel deposition on platinum single crystal electrodes has been investigated in solutions of different pH with cyclic voltammetry and CO charge displacement. Nickel deposition takes place on Pt(111) and Pt(110) in the low potential range, close to the hydrogen evolution and coupled with the hydrogen adsorption, for pH>3. No nickel deposition has been detected on Pt(100). The detailed reasons for such dependence on pH and crystallographic orientation remain unsolved at the present stage. Regarding the pH dependence, the increase of the pH allows separation of the nickel upd process from the hydrogen adsorption process and therefore, this could be one of the reasons for the more facile deposition process at higher pH values. In this regards, we have previously demonstrated that the potential of zero free charge (pzfc) of Pt(111) remains almost invariable with the pH in the SHE scale [22, 23]. Because measurements in this paper are presented in the RHE scale, charge becomes more negative as the pH is increased (for a given potential in the RHE scale), therefore facilitating the nickel adsorption. For Pt(110) there is no data for pH dependence of pzfc but we can consider measurements of the potential of maximum entropy (pme) as indication of the variation of the

pzfc for this surface[47]. In this case, a small shift of the pme (in the RHE scale) towards positive values when pH is increased of nearly 0.15 mV/pH unit would be also consistent with increasing amounts of negative charge that would favour nickel deposition. A second argument that can plausibly explain the observed trend with the pH implies the fact that nickel is coadsorbed with hydroxyl species, as deduced from the CO charge displacement experiments. In this case, increasing values of pH would increase the chemical potential of hydroxyl in solution, therefore favouring the codeposition process according to the following reaction:

$Ni^{2+} + n\ H_2O + (2\text{-}n)e \rightarrow Ni(OH)_n + n\ H^+$

Another intriguing fact is the absence of deposition on Pt(100) surface while the behaviour of Pt(111) and Pt(110) is rather similar. The latter observation indicates certain lack of sensibility to the long range order of the surface. In this regards it is worth recalling that Pt(110) may suffer a surface reconstruction to a (1x2) structure that results on the formation of (111) microfacets [48]. We could argue that such reconstruction is at the origin of the similarity between (111) and (110) surfaces. However, under the preparation conditions used in this work (fast cooling in Ar+H_2 mixture) it is usually assumed that (1x1) surface is formed. Therefore, additional investigation of the effect of surface preparation for the (110) surface would be required to shed light on this point. Regarding the lack of Ni adsorption on Pt(100) we can just speculate that the square arrangement of atoms is energetically unfavourable for Ni adsorption. Obviously, ab initio computer simulation would be necessary to clarify this point.

From the displaced charges, an estimation of nickel coverages has been possible, resulting a maximum coverage around 0.6 nickel per surface platinum atom. The formal partial charge number for nickel would be given by:

$$l_{Ni} = \frac{q_{Ni} - q_{OH}}{q_{111}\theta_{Ni}} = 2 - n$$

This would be the apparent charge involved in the Ni hydroxyl coadsorption. Unfortunatelly the dependence between *n* (number of adsorbed OH per Ni) and *m* (number of blocked Pt per Ni) given by equation (14) does not allow independent determination of both variables. Formal partial charge number for nickel deposition on polycrystalline platinum has been previously determined from EQCM measurements resulting a value around 1.2 [18]. Such value, significantly lower than 2, would be consistent with the hydroxyl coadsorption process detected in the present work.

Stripping of CO from the bimetallic Ni/Pt(111) surface has also been investigated with cyclic voltammetry, chronoamperometry and FTIRAS. At low potentials CO is be adsorbed on the nickel adlayers on bridge position. When the potential is scanned positively nickel adatoms are stripped from the surface and the CO is transferred to the underlaying platinum atoms. During this process, a small amount of CO is oxidised, probably through a bifunctional mechanism where nickel act as donor of OH species.

Transfer of the nickel adlayer to a free Ni^{2+} solution has been also attempted in the present work. These experiments show that nickel adsorption is a reversible process and nickel adlayers are not stable when Ni^{2+} is removed from the solution. However, covering the adlayer with CO increases its stability. Further research is in progress trying to transfer the nickel adlayers on platinum to solutions with higher pH to test their electrocatalytic properties under conditions where nickel adlayer would be stable. This method could offer the possibility to prepare nickel adlayers with well-defined and controlled coverage.

Acknowledgments:

The authors thankfully acknowledge financial support from the Ministerio de Economia, Industria y Competitividad (CTQ2016-76221-P and PEJ-2014-A-57942/PEJ-2014-P-00295).

References

[1] G. Kokkinidis, "Underpotential deposition and electrocatalysis", J. Electroanal. Chem., 201 (1986) 217-236.

[2] R. Parsons, T. Vandernoot, "The oxidation of small organic-molecules - A survey of recent fuel-cell related research", J. Electroanal. Chem., 257 (1988) 9-45.

[3] T. Bligaard, J.K. Norskov, "Ligand effects in heterogeneous catalysis and electrochemistry", Electrochim. Acta, 52 (2007) 5512-5516.

[4] V. Climent, N. García-Araez, J.M. Feliu, Clues for the Molecular-Level Understanding of Electrocatalysis on Single-Crystal Platinum Surfaces Modified by p-Block Adatoms, in: M.T.M. Koper (Ed.) Fuel Cells Catalysis. A Surface Science Approach, John Wiley & Sons, Inc., Hoboken, New Jersey, 2009, pp. 209-244.

[5] E. Leiva, T. Iwasita, E. Herrero, J.M. Feliu, "Effect of adatoms in the electrocatalysis of HCOOH oxidation. A theoretical model", Langmuir, 13 (1997) 6287-6293.

[6] A. Cuesta, "Atomic Ensemble Effects in Electrocatalysis: The Site-Knockout Strategy", ChemPhysChem, 12 (2011) 2375-2385.

[7] E. Herrero, L.J. Buller, H.D. Abruna, "Underpotential deposition at single crystal surfaces of Au, Pt, Ag and other materials", Chem. Rev., 101 (2001) 1897-1930.

[8] Z. Shi, S. Wu, J. Lipkowski, "Coadsorption of metal atoms and anions:Cu upd in the presence of SO 4 2-, Cl- and Br", Electrochim. Acta, 40 (1995) 9-15.

[9] V.R. Stamenkovic, B. Fowler, B.S. Mun, G.F. Wang, P.N. Ross, C.A. Lucas, N.M. Markovic, "Improved oxygen reduction activity on Pt3Ni(111) via increased surface site availability", Science, 315 (2007) 493-497.

[10] N. Danilovic, R. Subbaraman, D. Strmcnik, K.C. Chang, A.P. Paulikas, V.R. Stamenkovic, N.M. Markovic, "Enhancing the Alkaline Hydrogen Evolution Reaction Activity through the Bifunctionality of Ni(OH)2/Metal Catalysts", Angew. Chem. Int. Edit., 51 (2012) 12495-12498.

[11] R. Subbaraman, D. Tripkovic, K.C. Chang, D. Strmcnik, A.P. Paulikas, P. Hirunsit, M. Chan, J. Greeley, V. Stamenkovic, N.M. Markovic, "Trends in activity for the water electrolyser reactions on 3d M(Ni,Co,Fe,Mn) hydr(oxy)oxide catalysts", Nat. Mater., 11 (2012) 550-557.

[12] I. Ledezma-Yanez, W.D.Z. Wallace, P. Sebastian-Pascual, V. Climent, J.M. Feliu, M.T.M. Koper, "Interfacial water reorganization as a pH-dependent descriptor of the hydrogen evolution rate on platinum electrodes", Nat Energy, 2 (2017).

[13] K. Franaszczuk, J. Sobkowski, "Nickel adsorption on a platinized platinum-electrode", Surf. Sci., 204 (1988) 530-536.

[14] A.A. El-Shafei, "Study of nickel upd at a polycrystalline Pt electrode and its influence on HCOOH oxidation in acidic and nearly neutral media", J. Electroanal. Chem., 447 (1998) 81-89.

[15] M. Chatenet, R. Faure, Y. Soldo-Olivier, "Nickel-underpotential deposition on Pt(110) in sulphate-containing media", J. Electroanal. Chem., 580 (2005) 275-283.

[16] M. Chatenet, Y. Soldo-Olivier, E. Chainet, R. Faure, "Understanding CO-stripping mechanism from Ni-UPD/Pt(110) in view of the measured nickel formal partial charge number upon underpotential deposition on platinum surfaces in sulphate media", Electrochim. Acta, 53 (2007) 369-376.

[17] M. Chatenet, Y. Soldo-Olivier, E. Chainet, R. Faure, "Electrochemical quartz crystal microbalance determination of nickel formal partial charge number during nickel-underpotential deposition on platinum in sulphate media", Electrochem. Commun., 9 (2007) 1463-1468.
[18] M. Chatenet, "Electrochemical Quartz Crystal Microbalance Determination of Nickel Formal Partial Charge Number as a Function of the Electrode Potential upon Nickel Underpotential Deposition on Platinum in Sulfuric Medium", Electrocatalysis, 6 (2015) 382-389.
[19] J. Clavilier, D. Armand, S.G. Sun, M. Petit, "Electrochemical adsorption behaviour of platinum stepped surfaces in sulphuric acid solutions ", J. Electroanal. Chem., 205 (1986) 267-277.
[20] C. Korzeniewski, V. Climent, J.M. Feliu, Electrochemistry at Platinum Single Crystal Electrodes, in: A.J. Bard, C. Zoski (Eds.) Electroanalytical Chemistry: A Series of Advances, Vol 24, vol. 24, 2012, pp. 75-169.
[21] V. Climent, R. Gómez, J.M. Feliu, "Effect of increasing amount of steps on the potential of zero total charge of Pt(111) electrodes", Electrochim. Acta, 45 (1999) 629-637.
[22] R. Martinez-Hincapie, P. Sebastian-Pascual, V. Climent, J.M. Feliu, "Exploring the interfacial neutral pH region of Pt(111) electrodes", Electrochem. Commun., 58 (2015) 62-64.
[23] R. Rizo, E. Sitta, E. Herrero, V. Climent, J.M. Feliu, "Towards the understanding of the interfacial pH scale at Pt(111) electrodes", Electrochim. Acta, 162 (2015) 138-145.
[24] R.M. Arán-Ais, M.C. Figueiredo, F.J. Vidal-Iglesias, V. Climent, E. Herrero, J.M. Feliu, "On the behavior of the Pt(100) and vicinal surfaces in alkaline media", Electrochim. Acta, 58 (2011) 184-192.
[25] J.M. Feliu, A. Rodes, J.M. Orts, J. Clavilier, "The problem of surface order of pt single-crystals in electrochemistry", Pol. J. Chem., 68 (1994) 1575-1595.
[26] A.V. Rudnev, T. Wandlowski, "An influence of pretreatment conditions on surface structure and reactivity of Pt(100) towards CO oxidation reaction", Russ. J. Electrochem., 48 (2012) 259-270.
[27] A. AlAkl, G.A. Attard, R. Price, B. Timothy, "Voltammetric and UHV characterization of the (1x1) and reconstructed hex-R0.7º phases of Pt(100)", J. Electroanal. Chem., 467 (1999) 60-66.
[28] N. Garcia-Araez, V. Climent, P. Rodríguez, J.M. Feliu, "Thermodynamic analysis of (bi)sulphate adsorption on a Pt(111) electrode as a function of pH", Electrochim. Acta, 53 (2008) 6793-6806.
[29] B. Braunschweig, W. Daum, "Superstructures and Order/Disorder Transition of Sulfate Adlayers on Pt(111) in Sulfuric Acid Solution", Langmuir, 25 (2009) 11112-11120.
[30] A.M. Funtikov, U. Stimming, R. Vogel, "Anion adsorption from sulfuric acid solutions on Pt(111) single crystal electrodes", J. Electroanal. Chem., 428 (1997) 147-153.
[31] D. Strmcnik, K. Kodama, D. van der Vliet, J. Greeley, V.R. Stamenkovic, N.M. Markovic, "The role of non-covalent interactions in electrocatalytic fuel-cell reactions on platinum", Nature Chem., 1 (2009) 466-472.
[32] C. Stoffelsma, P. Rodriguez, G. Garcia, N. Garcia-Araez, D. Strmcnik, N.M. Markovic, M.T.M. Koper, "Promotion of the Oxidation of Carbon Monoxide at Stepped Platinum Single-Crystal Electrodes in Alkaline Media by Lithium and Beryllium Cations", J. Am. Chem. Soc., 132 (2010) 16127-16133.
[33] A. Berna, V. Climent, J.M. Feliu, "New understanding of the nature of OH adsorption on Pt(111) electrodes", Electrochem. Commun., 9 (2007) 2789-2794.
[34] M. Chatenet, Y. Soldo-Olivier, E. Chainet, R. Faure, "Understanding CO-stripping mechanism from NiUPD/Pt(1 1 0) in view of the measured nickel formal partial charge number upon underpotential deposition on platinum surfaces in sulphate media", Electrochim. Acta, 53 (2007) 369-376.

[35] V. Climent, N. Garcia-Araez, E. Herrero, J. Feliu, "Potential of zero total charge of platinum single crystals: A local approach to stepped surfaces vicinal to Pt(111)", Russ. J. Electrochem., 42 (2006) 1145-1160.
[36] R. Martinez-Hincapie, P. Sebastian-Pascual, V. Climent, J.M. Feliu, "Investigating interfacial parameters with platinum single crystal electrodes", Russ. J. Electrochem., 53 (2017) 227-236.
[37] V. Climent, R. Gómez, J.M. Orts, A. Aldaz, J.M. Feliu, The potential of zero total charge of single-crystal electrodes of platinum group metals, in: C. Korzeniewski, B.E. Conway(Eds.) The Electrochemical Society Proceedings (Electrochemical Double Layer), The Electrochemical Society, Inc., Pennington, NJ, 1997, pp. 222-237.
[38] N.P. Lebedeva, M.T.M. Koper, J.M. Feliu, R.A. van Santen, "Mechanism and kinetics of the electrochemical CO adlayer oxidation on Pt(111)", J. Electroanal. Chem., 524 (2002) 242-251.
[39] N.M. Markovic, B.N. Grgur, C.A. Lucas, P.N. Ross, "Electrooxidation of CO and H_2/CO mixtures on Pt(111) in acid solutions", J. Phys. Chem. B, 103 (1999) 487-495.
[40] A. López-Cudero, A. Cuesta, C. Gutiérrez, "Potential dependence of the saturation CO coverage of Pt electrodes: The origin of the pre-peak in CO-stripping voltammograms. Part 1: Pt(1 1 1)", J. Electroanal. Chem., 579 (2005) 1-12.
[41] A. Rodes, R. Gómez, J.M. Feliu, M.J. Weaver, "Sensitivity of compressed carbon monoxide adlayers on platinum(III) electrodes to long-range substrate structure: Influence-of monoatomic steps", Langmuir, 16 (2000) 811-816.
[42] M. Zhao, K.L. Wang, D.A. Scherson, "In situ Potential Difference Fourier-Transform Infrared Reflection Absorption Spectroscopic studies of the electrochemical oxidation of adsorbed carbon-monoxide on nickel in alkaline-solutions", J. Phys. Chem., 97 (1993) 4488-4490.
[43] R.B. Bailey, T. Iri, P.L. Richards, "Infrared spectra of carbon monoxide on evaporated nickel films: A low temperature thermal detection technique", Surf. Sci., 100 (1980) 626-646.
[44] M. Primet, J.A. Dalmon, G.A. Martin, "Adsorption of CO on well-defined Ni-SiO2 catalysts in 195-373 K range studied by infrared spectroscopy and magnetic methods", J. Catal., 46 (1977) 25-36.
[45] M.W. Severson, C. Stuhlmann, I. Villegas, M.J. Weaver, "Dipole-dipole coupling effects upon infrared-spectroscopy of compressed electrochemical adlayers - application to the Pt(111)/CO system", J. Chem. Phys., 103 (1995) 9832-9843.
[46] I. Villegas, M.J. Weaver, "Carbon-monoxide adlayer structures on platinum(111) electrodes - a synergy between in-situ scanning-tunneling-microscopy and infrared-spectroscopy", J. Chem. Phys., 101 (1994) 1648-1660.
[47] N. Garcia-Araez, V. Climent, J. Feliu, "Potential-Dependent Water Orientation on Pt(111), Pt(100), and Pt(110), As Inferred from Laser-Pulsed Experiments. Electrostatic and Chemical Effects", J. Phys. Chem. C, 113 (2009) 9290-9304.
[48] C.A. Lucas, N.M. Markovic, P.N. Ross, "Surface structure and relaxation at the Pt(110)/electrolyte interface", Phys. Rev. Lett., 77 (1996) 4922-4925.

Highlights

Nickel underpotential deposition on platinum single crystal electrodes is investigated.

Nickel upd is observed on Pt(111) and Pt(110) for pH>3.

CO charge displacement on Pt(111)/Ni suggest that the adlayer is covered with OH.

Coulometric analysis is used to deduce the stoichiometry of the deposited adlayer.

FTIRRAS investigation of CO/Ni/Pt(111) detect the displacement of CO from Ni to Pt after Ni stripping.